Microscopic Residual Stress Caused by the Mechanical Heterogeneity in the Lamellar Unit of the Porcine Thoracic Aortic Wall*

Takeo MATSUMOTO**,****, Taisuke GOTO***,**** and Masaaki SATO****

The opened-up configuration of the artery wall has long been assumed to be stress-free. This is questionable at a microscopic level: The aortic media has a laminated structure consisting of an elastic lamina (EL) and a smooth muscle-rich layer (SML). The ELs are corrugated in the opened-up configuration, suggesting their buckling. We found that the ELs were much stiffer than the SMLs from a radial compression test of the porcine aortas. Such mechanical heterogeneity may cause microscopic residual stress, which is hardly released by the radial cutting except in the area close to the cut surface, where the release may cause hills and valleys. To check this hypothesis, we measured the topography and the stiffness distribution of the cut surface of the aortas with a scanning micro indentation tester to find stiff hills (EL) and soft valleys (SML). Residual stress estimated from the measurements was almost comparable to the conventionally estimated values and was large enough to cause the buckling. Fairly large stress may still reside in the opened-up aortic wall.

Key Words: Biomechanics, Material Testing, Stress Analysis, Compression Test, Indentation Test, Buckling, Surface Topography

1. Introduction

It is well known that if you cut a ring-like segment of an aorta usually, it springs open to become an arc. It has been pointed out that this happens because circumferential stress in the aortic wall distributes uniformly in the radial direction in vivo, and as a result, the segment at no load has compressive residual stress near the inner wall and tensile near the outer as happens in a thick-walled cylinder[1]. The opened-up configuration has long been assumed to be stress-free since the importance of residual stress was pointed out[2),(3)]. This assumption would be correct if the aortic wall is homogeneous. However, the wall is heterogeneous in a microscopic level: its media has a laminated structure called lamellar unit[4] which is a pair of elastic lamina (EL) composed of elastin and a smooth muscle-rich layer (SML). Elastic modulus of elastin is about 0.6 MPa[5], while that of the smooth muscle cell is in an order of 0.01 MPa in the relaxed state[6]. Thus, the EL might be much stiffer than the SML.

If the EL is stiffer than the SML and if the circumferential stress of the two layers is the same in the in vivo condition as happens in the aortic wall in a macroscopic level, compressive residual stress should appear in the EL while it is still tensile in the SML (Fig. 1 (a)). Such residual stresses may hardly be released by the radial cutting except in the area close to the cut surface, and the release may cause hills and valleys on the surface (Fig. 1 (b)). The ELs are often corrugated in the histological sections of the opened-up segments (Fig. 2). It is hard to believe that the ELs remain wavy in their stress-free state. Thus, the corrugation may indicate the buckling due to compressive residual stress.

In this study, we first compared the stiffness of the EL and SML in the porcine thoracic aortas by measuring the change in thickness of the two layers during radial compression, and found that the EL is stiffer than the SML. We then measured the surface topography and the distribution of the stiffness on the cut surface of the aortas with a newly developed scanning micro indentation tester (SMIT) to find that the cut surface shows hill and valley pattern. And finally we estimated the residual stress and

* Received 5th January, 2004 (No. 04-4003)

** Present affiliation: Dep. Mech. Eng., Nagoya Inst. Tech., Gokiso-cho, Showa-ku, Nagoya, Aichi 466–8555, Japan. E-mail: takeo@nitech.ac.jp

*** Present affiliation: Shimadzu Corp., Nagoya, Japan

**** Tohoku Univ., Aoba-yama 01, Sendai 980–8579, Japan

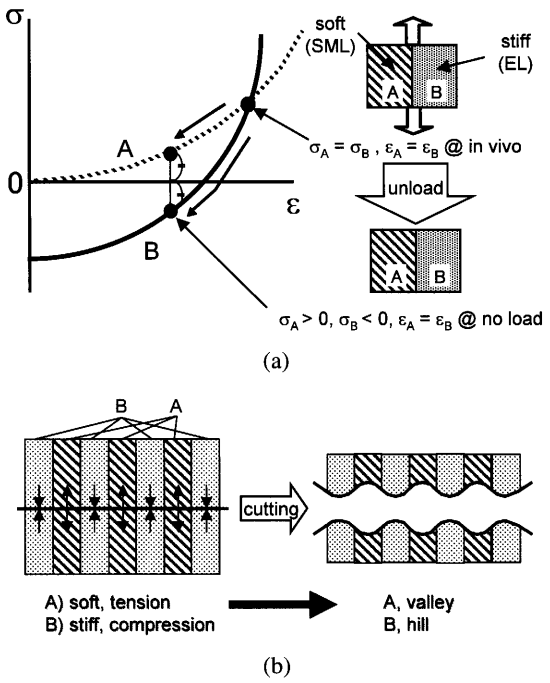

Fig. 1 Schematic diagrams on residual stress caused by material heterogeneity (a) and hill and valley pattern caused by such residual stress (b). The thicknesses of the two layers are assumed to be the same for simplicity.

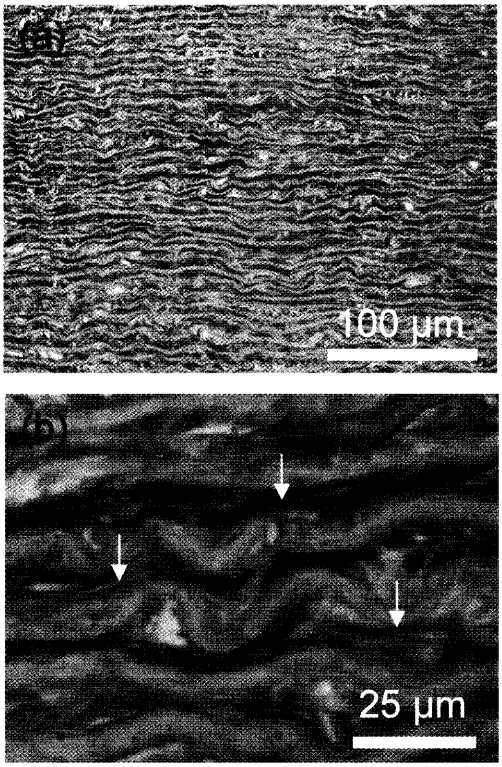

Fig. 2 A section of the porcine thoracic aorta stained with Azan. Corrugated elastic laminae are observed as white wavy lines. Note that smooth muscles between the laminae (red) remain stretched (white arrows).

strain with a 2D simplified model, and found that such residual components were almost comparable to those estimated in the ring-like segments in no load condition and were large enough to cause the bucking of the ELs.

2. Radial Compression Test: Estimation of Elastic Properties in the Lamellar Unit

2.1 Principle of the measurement

Wall thickness decreases when a segment of an artery is compressed radially. If the EL is stiffer than the SML, compressive strain is smaller in the EL and larger in the SML than in the whole wall. The ratio of the strain be-

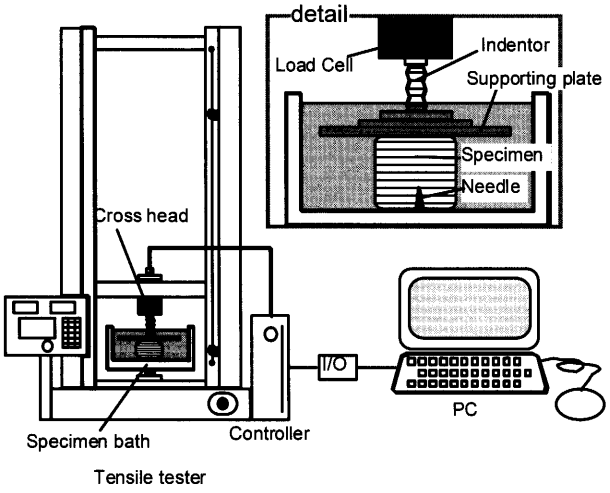

Fig. 3 Experimental set up for the radial compression test.

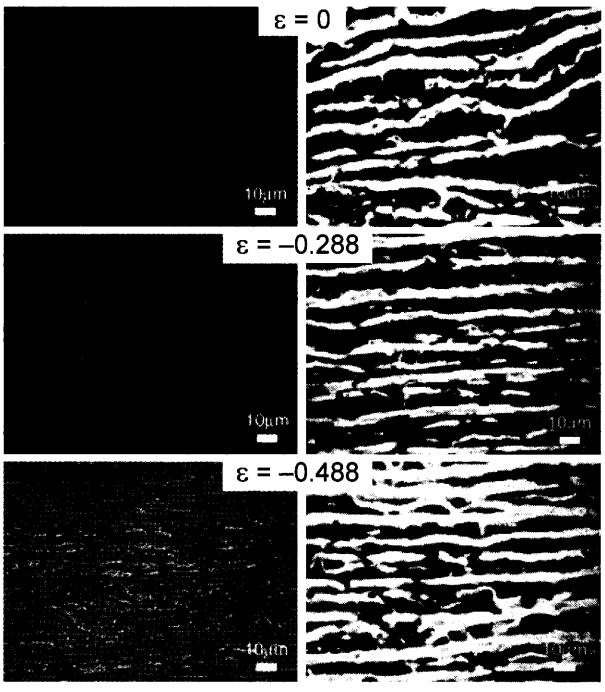

Fig. 4 Examples of histological sections of formalin-fixed specimens subjected to various levels of radial compressive strain.

tween the EL and the SML corresponds to the inverse ratio of the elastic modulus between the two layers. In this series of experiment, changes in thickness of the EL and SML during radial compression were measured in the histological sections of the specimens fixed during radial compression.

2.2 Specimens

We used porcine aortas as a test model. Three tubular segments of descending thoracic aortas were obtained at a local slaughterhouse. After adventitia was carefully removed, 5 short tubular segments about 15 mm in length were obtained in the area between the end of the aortic arch and the 6th intercostal artery. The segments were then cut longitudinally at the root of the intercostal arteries. Three to four 9 mm square specimens (1 – 3 mm thick) were cut out from each segment with a special jig.

2.3 Radial compression test

Figure 3 shows the experimental setup used for the radial compression test. A tensile tester (AGS-50D Type 3, Shimadzu, Japan) was used in a compression mode. Standard jigs for tensile test were replaced with an indenter and a specimen bath. The indenter has a 20 mm square aluminum plate (2 mm thick) at its tip to compress the specimen. The specimen bath is 60 mm square with the depth of 15 mm. To prevent the slippage of the specimen during compression, a 1 mm long acupuncture needle of 0.2 mm diameter (Spinex 02×3, Seirin, Japan) was fixed at the center of its bottom.

Each of the specimens was compressed in the radial direction at the rate of 0.5 mm/min in a physiological saline solution at room temperature to various strain levels (from −0.1 to −0.5). The specimen was then immediately fixed with formalin for at least 6 h while being compressed. The compression was released after the fixation and histological sections perpendicular to the longitudinal direction were obtained to measure the thickness of the EL and the SML. Specimens adjacent to each compressed specimen were fixed without compression to obtain control sections.

2.4 Measurement of the thickness in the EL and SML

Histological sections were stained with Hematoxylin-Eosin (HE). When stained with HE, the elastin becomes fluorescent (excitation: 480 – 550 nm, emission: > 590 nm), and the EL can be observed clearly as shown in Fig. 4. Eight-bit gray-scale fluorescent images (800× 600 pixels, corresponding to 160×120 μm) of the EL were taken with a digital microscope camera (Polaroid, U.S.A.) mounted to a fluorescent microscope (BX51, Olympus, Japan) and fed to a computer (Macintosh PowerBookG3, Apple computer, U.S.A.) for an image analysis with NIH image (NIH, U.S.A.). The image was binarized for the EL and the relative area occupied by the EL (area in white) $\%A_{EL}$ and the SML (area in black) $\%A_{SML}$ were obtained. The mean thickness of the EL and the SML (t^f_{EL} and t^f_{SML}, respectively) were obtained from the relative areas, the number of the lamellae, and the magnification of the image. The thickness of each specimen was measured in sub-intimal, mid-wall, and sub-adventitial regions. Five images taken randomly in each region were analyzed.

2.5 Consideration of elastic recoil

Soft biological tissues fixed with formalin are not completely rigid. They remain more or less elastic even after the fixation. The degree of fixation is different among the components of the soft tissues. Among them, elastin is known to be less fixable. Thus, the fixed aortic specimens increase their thickness after the compressive stress is removed, and the thicknesses measured in the previous section, i.e., those measured after the compressive stress is removed have to be converted to the values during compression. Such thicknesses were obtained considering the mechanical properties of formalin-fixed tissues. To know the mechanical properties of formalin-fixed elastin, a denatured ligamentum nuchae of a goat was used. The ligament was boiled in water at 100°C for 1 h to remove collagen completely[5], sliced in the longitudinal (fiber) direction into 2 – 3 mm thick specimens, and fixed with formalin for 6 h. Compression test was then performed for 4 specimens similarly to the section 2.3 to obtain the stress-strain relationship of the elastin, i.e., EL fixed with formalin (Fig. 5). The compression test was also performed for 4 formalin-fixed specimens of the porcine aorta. Stress-strain relationship of the formalin-fixed SML was obtained by combining that of the fixed whole vessel wall and that of the fixed EL.

As shown in the appendix, the thicknesses of the EL and SML during radial compression (t^c_{EL} and t^c_{SML}, respectively) were obtained assuming incompressibility of the wall as:

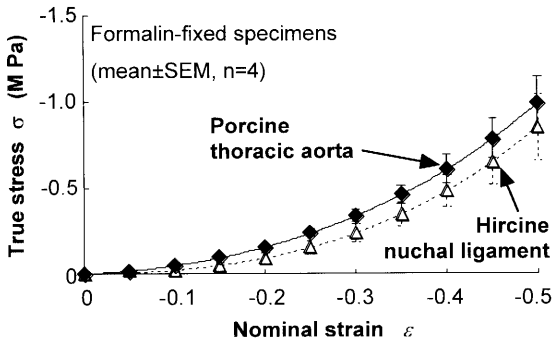

Fig. 5 Stress-strain curves of formalin-fixed specimens. The curves were fitted with fourth order polynomial: $\sigma = -1\,721\varepsilon^4 + 1\,309\varepsilon^3 - 2\,416\varepsilon^2 + 225\varepsilon$ ($R^2 = 1.000$) for the nuchal ligament and $\sigma = 1\,373\varepsilon^4 + 5\,735\varepsilon^3 - 651\varepsilon^2 + 110\varepsilon$ ($R^2 = 1.000$) for the thoracic aorta.

$$t_{EL}^{c}=\frac{\frac{t_w^c}{t_w^f}(t_{EL}^f+t_{SML}^f)-t_{SML}^f(1-\gamma(\varepsilon_w^{c*}))}{1+\frac{t_{SML}^f}{t_{EL}^f}\gamma(\varepsilon_w^{c*})}, \quad (1)$$

$$t_{SML}^{c}=t_{SML}^{f}\left\{\gamma(\varepsilon_w^{c*})\left(\frac{t_{EL}^c}{t_{EL}^f}-1\right)+1\right\}, \quad (2)$$

$$\gamma(\varepsilon_w^{c*})=\frac{E_{EL}^f(\varepsilon_{EL}^{c*})}{E_{SML}^f(\varepsilon_{SML}^{c*})}, \quad (3)$$

where t_w^c and t_w^f are the whole wall thicknesses of the specimen during compression and after fixation and unloading, respectively, and E_{EL}^f and E_{SML}^f are the secant elastic moduli of the EL and SML after fixation, respectively. The ε_i^{c*} ($i = EL$, SML, or w) indicates the nominal strain during compression with respect to the unloaded state after fixation, i.e., $\varepsilon_i^{c*}=t_i^c/t_i^f-1$.

Strains during compression with respect to the initial state, i.e., state before the radial compression, were obtained as:

$$\varepsilon_w=\frac{t_w^c-t_w}{t_w}, \quad \varepsilon_{EL}=\frac{t_{EL}^c-t_{EL}}{t_{EL}}, \quad \varepsilon_{SML}=\frac{t_{SML}^c-t_{SML}}{t_{SML}}, \quad (4)$$

where t without superscript indicates the thickness in the initial state measured before compression test (t_w) and measured in each control specimen fixed without compression (t_{EL} and t_{SML}).

2.6 Difference in the mechanical properties between the elastic and the smooth muscle layer

Example of the thicknesses in a no-load and a compressed specimen is shown in Fig. 6. The thickness decreased in both layers in the compressed specimen (b). The decrease was much larger in the SML than the EL, suggesting the EL is stiffer than the SML. Figure 7 summarizes the change in strain due to radial compression. Although the scatter was large, strain in the SML was compressive (negative) in all cases and was generally higher than the strain applied to the whole wall. Compressive strain in the EL was generally lower than the whole wall strain and was tensile (positive) in about 30% of the specimens. The straight lines are regression lines crossing the origin for the EL and SML. The ratio of their slope corresponds to the ratio of the compliance of the two layers. The slope was about 2.5 times higher in the SML than in the EL, indicating that the compressive elastic modulus is 2.5 times higher in the elastic lamina than in the smooth muscle-rich layer.

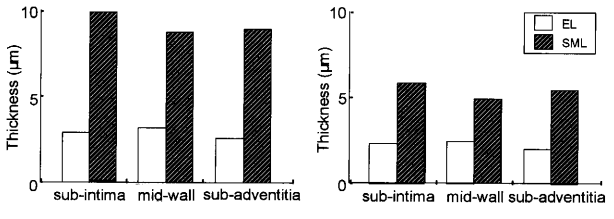

(a) $\varepsilon=0$ (b) $\varepsilon=-0.31$

Fig. 6 Thickness of elastic lamina (EL) and smooth muscle layer (SML) in a no-load (a) and a compressed (b) porcine thoracic aorta.

3. Indentation Test: Measurement of Surface Topography and Stiffness Distribution

3.1 Scanning micro indentation tester (SMIT)

Details of the SMIT have been reported elsewhere[7]. Schematic diagram of the SMIT is shown in Fig. 8. It is a tester to measure the surface topography and stiffness distribution of a specimen surface by pressing a cantilever tip against the specimen while scanning it like an atomic force microscope. The cantilever was made from a micro glass plate of 65 mm×1 mm×0.15 mm (Asahi Techno Glass Corp., Japan) by pulling it with a pipette puller (PP-83, Narishige Co., Ltd., Japan) to make its tip diameter 3–5 μm and bending it with a microforge (MF-90, Narishige Co., Ltd., Japan) at right angle at the point 4 mm from the tip. The cantilever was driven by a PZT actuator (AE505D1, Tokin Corp., Japan) and the displacement of its tip was measured with a confocal laser displacement meter (LT8100, Keyence Corp., Japan). The measurement

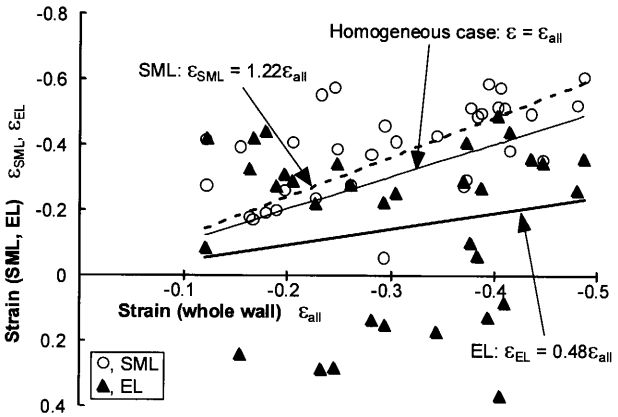

Fig. 7 Difference in strain between EL and SML during radial compression.

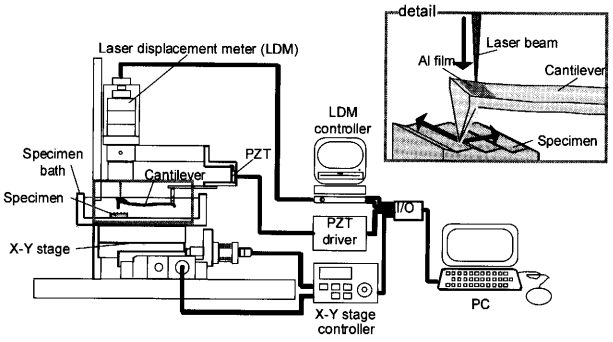

Fig. 8 Schematic diagram of the scanning micro indentation tester (SMIT).

was done in a bath filled with a physiological saline solution at room temperature. The specimen bath was set on a motor-driven XY stage (MINI60X, Sigma Koki Co., Ltd., Japan) to scan the point of measurement. The contact point was determined at the point where the cantilever began deflecting, and a stiffness index α was obtained as the initial slope of the indentation-deflection curve. The index α was converted to elastic modulus E with the following formula obtained by calibrating the tester with silicone elastomers with known elastic moduli:

$$E\,[\mathrm{kPa}] = 1.88\exp(2.54\alpha) \qquad (5)$$

The PZT actuator and the X – Y stage were controlled with a PC (DynaBook Satellite 2210 SA50C/4C8, Toshiba, Japan) equipped with an I/O board (DAQ Card-1200, National Instruments, U.S.A.) Data were measured and analyzed on the same PC. Control of the system and the data measurement were performed with a measurement and automation software LabVIEW (version 5.0; National Instruments, U.S.A.).

3.2 Method of the measurement

Rectangular specimens of 5×10 mm (2 – 3 mm thick) were excised from porcine descending thoracic aortas as described in section 2.2. Macroscopic residual stresses

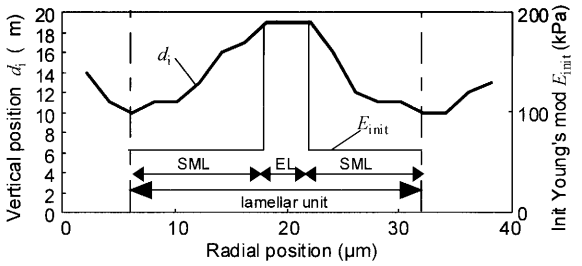

Fig. 10 An example of surface topology measured with the SMIT in a lamellar unit of a porcine aorta and corresponding distribution of the elastic modulus assumed from the measurements and histology.

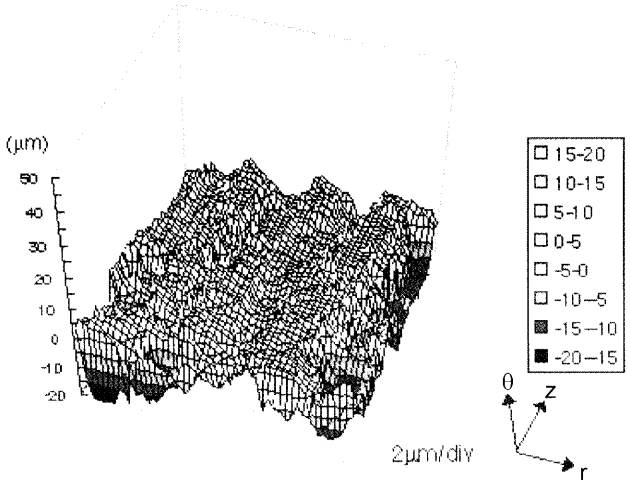

(a) Surface topography

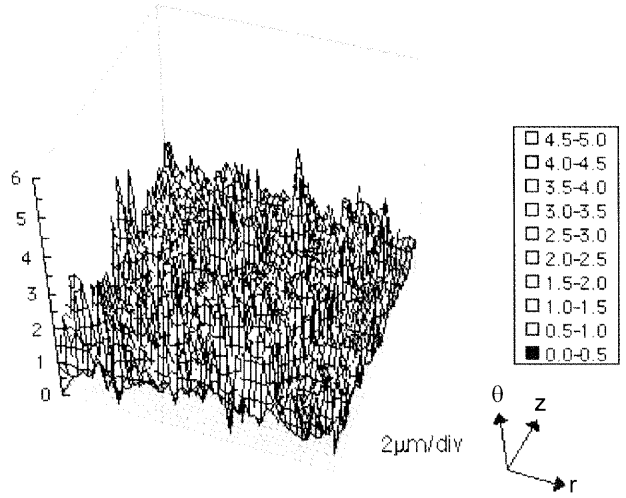

(b) Stiffness distribution

Fig. 9 A set of data obtained with the SMIT for a section perpendicular to the circumferential direction of a porcine thoracic aorta.

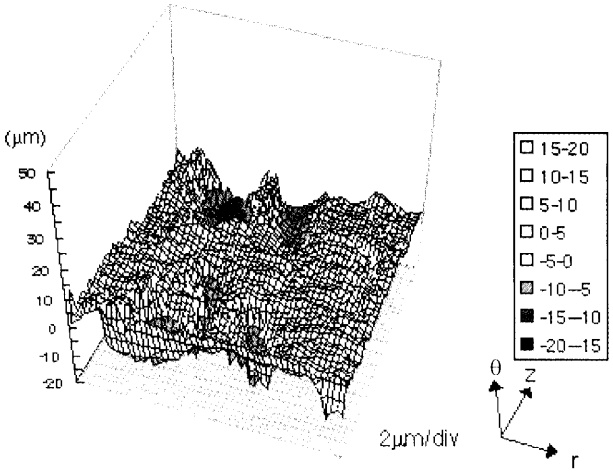

(a) $d = 80\,\mu\mathrm{m}$

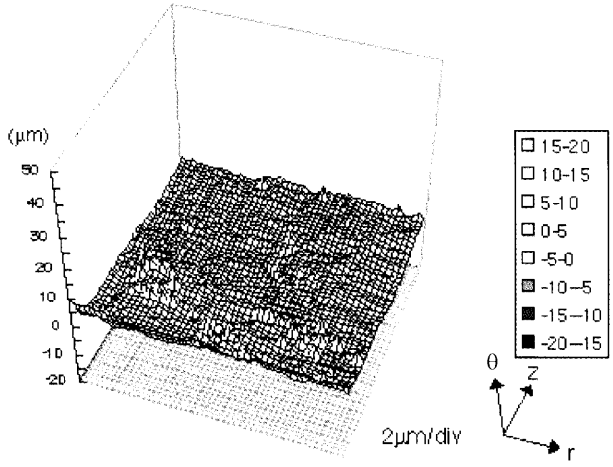

(b) $d = 70\,\mu\mathrm{m}$

Fig. 11 Surface topography measured after thin layer with thickness d was sliced off from the surface of formalin-fixed specimens.

are removed during excision. Each of the specimens was embedded in an agar gel with low gelling temperature (30–31°C, Nacalai Tesque, Japan) and sliced with a tissue sectioner (Microslicer DTK-1500, Dosaka EM Co., Ltd., Japan) in the saline to obtain the surface perpendicular to the circumferential or axial directions of the aorta. The specimen with its bath was then mounted on the XY stage of the SMIT for the measurement. The indentation test was performed in the area of 100 μm×100 μm at 2 μm-intervals to obtain the surface topography and the stiffness distribution.

3.3 Surface topography and stiffness distribution

An example of the surface topography and the stiffness distribution is shown in Fig. 9. The surface of the section shows hill and valley pattern perpendicular to the radial direction. The average distance between the peaks and the peak height were ~ 25 and ~ 8 μm, respectively. The elastic modulus estimated from α was ~ 180 kPa at the peak and ~ 52 kPa at the bottom. As shown in the previous chapter, we found that the elastic modulus of EL is 2.5 times higher than that of SML. Thus, we suppose the hill must be EL and the valley SML, i.e., EL may be compressed and SML stretched in the lamellar unit.

4. Estimation of Residual Stress and Strain

4.1 Model and assumptions

The stress distribution required to restore the hill and valley pattern to the plane where the specimen was cut corresponds to the residual stress distribution. Such distribution was estimated on a 2D simplified model based on the surface topography and an idealized distribution of the elastic modulus shown in Fig. 10. Following assumptions were made: 1) the thickness of the EL and the SML are 4 and 22 μm, respectively; 2) lamellar unit is made of thirteen 2-μm-thick layers (two for the EL and eleven for the SML); 3) the height of each layer l_i equals to its vertical position d_i shown in Fig. 10 plus an offset δ, i.e., $l_i = d_i + \delta$; 4) EL and SML are linearly elastic with the elastic modulus E_i of 180 and 52 kPa, respectively; 5) residual stress σ_i is released upon cutting from the cut surface to the depth l_o, i.e., $\sigma_i = E_i(l_i - l_o)/l_o$; 6) shear stress and lateral deformations are negligible. The offset δ was obtained so as to make the sum of the residual stress zero, i.e., $\Sigma\sigma_i = 0$. To estimate the depth l_o, thin slices with various thicknesses were removed from the surface of formalin-fixed specimens with the Microslicer while measuring surface topography with the SMIT. The height difference between hills and valleys decreased dramatically when the thickness was smaller than 70 μm (Fig. 11). Thus, we roughly estimated l_o to be less than 70 μm.

4.2 Residual stress and strain in the lamellar unit

Residual stress and strain in the lamellar unit shown in Fig. 10 was analyzed for l_o = 30 and 60 μm (Fig. 12). The model analysis showed that the residual stress and

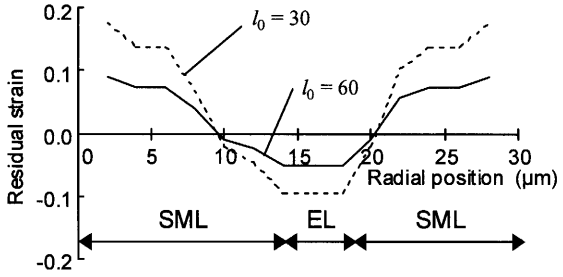

(a) Residual strain

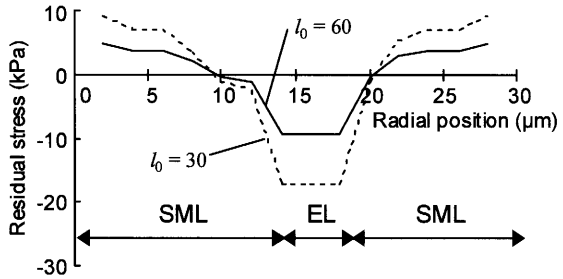

(b) Residual stress

Fig. 12 Residual stress and strain distributions in the lamellar unit shown in Fig. 10. Two cases are calculated for l_o = 30 and 60 μm.

strain increased with the decrease in l_o, and that the residual stress is at least −10 kPa for the EL and 3 kPa for the SML and the residual strain is at least −6% for the EL and 5% for the SML. These values are almost comparable to those conventionally estimated in the ring-like segment of the aortas in no load condition[8].

4.3 Estimation of buckling stress of the EL

Let us assume that the compressive residual stress in the EL causes buckling and the EL becomes corrugated with the spatial period of p. The critical stress causing the buckling is obtained from the Euler buckling formula for a plate of thickness h and length p, fixed at both ends:

$$\sigma_c = \frac{\pi^2 E h^2}{3p^2}. \tag{6}$$

Histological observation revealed that the spatial period l was around 50 μm and the thickness $h \sim 4$ μm. The elastic modulus of the EL without bucking can be assumed to be that of the elastin, 0.6 MPa. The buckling stress was thus estimated to be ~ 10 kPa, which is almost comparable to the estimation of the compressive residual stress in the EL.

5. Discussion

There have been a lot of studies on the residual stress and strain in the artery wall. Most of them assumed that the wall is homogeneous[1),(8),(9)], and those taking the heterogeneity of the wall material into consideration are few. Vossoughi et al.[10] found that the opening angle was much larger in the inner half layer than the outer half layer of the ring-like segments of the bovine thoracic aortas. Sim-

ilar phenomenon was observed by Greenwald et al.[11] Rachev[12] studied the stress distribution in the artery wall considering the artery to be a thick-walled two-layer tube. Recently, we studied the stress and strain distribution in the artery wall consisted of layers with different elastic modulus and opening angle[13]. However, heterogeneity considered in these studies remained in the macroscopic level and none of them considered the heterogeneity based on the histology.

In this study, we paid special attention to the microscopic heterogeneity and estimated the mechanical properties of the EL and SML by the radial compression test to find that the EL is 2.5 times stiffer than the SML. Generally speaking, residual stress tends to appear in a body consisted of the materials with different elastic properties. Thus, we measured the topography and the stiffness distribution of the cut surface, and found that the EL was in compression and SML in tension even in the state conventionally assumed to be stress-free.

The existence of the compressive residual stress in the EL and tensile in the SML can be supported by a close examination of the histological sections: As shown in Fig. 2, the ELs are usually corrugated even in a specimen whose macroscopic residual stress has been removed by the radial cutting, while the filaments in the smooth muscle cells in the SML remain stretched. It is hard to believe that the corrugated ELs are in a stress-free state. Furthermore, according to scanning electron microscopic observation of the 3D architecture of the elastic tissue isolated from the medial wall with formic acid treatment[14], the elastic laminae are straight and not corrugated. Thus, the corrugation may be the buckling of the ELs due to the compressive residual stress.

Compressive residual stress in the stiffer layer and tensile in the softer layer may indicate that the stress and/or strain is same in the two layers in a loaded state (Fig. 1). If such loaded state is close to the in vivo state, stress distribution is uniform not only in a macroscopic level but also in a microscopic level. This would be a very interesting hypothesis. At this point, however, it is very difficult to check this hypothesis, because we do not have a method to know the stress-strain relationship of the EL and SML in a wide stain range. Development of such a method is eagerly awaited.

There are several limitations to this study. First, we could not exclude the possibility that the surface we obtained is not completely flat. Cytoplasm of the smooth muscle cells crossing the cutting plane may dissolve into the saline solution during cutting. Uncontrollable slight deformation of the specimen during preparation may widen the soft smooth muscle layer. All of these changes may cause a dent in the SML. However, the hill and valley pattern was observed even in the specimens cut after formalin fixation. Furthermore, the corrugation of the ELs may indicate that they are being compressed in the unloaded wall. Although we could not control the above factors, we believe that the elastic lamina is in compression and the smooth muscle-rich layer in tension in the excised tissue.

The method of the stress analysis would be another limitation. We used a simple linear 2D model neglecting the shear force between the layers. Instead, we introduced the depth l_o to which residual stress is released upon cutting. We measured l_o experimentally and found it was smaller than 70 μm. The depth might be close to the thickness of the lamellar unit, i.e., ~ 30 μm from Saint-Venant's principle. The analysis showed that the smaller the l_o is, the larger the residual stress becomes, and the residual components were almost comparable to those of macroscopic components even in the largest l_o. The residual stress may be even higher if you assume nonlinear mechanical properties of the layers. Furthermore, the compressive residual stress was large enough to induce the buckling of the ELs. These results indicate that fairly large stress and strain may still reside in the macroscopically stress-free tissue. We need to study the residual stress and strain distribution in detail with a finite element analysis. Microscopic viewpoint is necessary to reveal the mechanical environment of the smooth muscle cells in the aortic media.

Acknowledgment

This work was supported in part by Grant-in-Aid from the Ministry of Education, Science and Culture in Japan (T. Matsumoto, Nos. 13450040, 14655040, and 15086209).

Appendix A: Deviation of Eqs. (1) – (3)

Assuming that the ratio of the wall thickness during compression to that after fixation and unloading t_w^c/t_w^f is equal to the corresponding ratio of the lamellar unit thickness $(t_{EL}^c + t_{SML}^c)/(t_{EL}^f + t_{SML}^f)$, we obtain:

$$t_w^c : t_w^f = (t_{EL}^c + t_{SML}^c) : (t_{EL}^f + t_{SML}^f). \tag{A.1}$$

Stress-strain relationships of the formalin-fixed EL and SML can be expressed with the secant moduli $E_i^f(\varepsilon_i^*)$ as:

$$\sigma_i(\varepsilon_i^*) = E_i^f(\varepsilon_i^*) \cdot \varepsilon_i^*, \quad (i = EL,\ SML), \tag{A.2}$$

where ε_i^* is the nominal strain with respect to the unloaded state after formalin fixation (denoted as ε in Fig. 5). Considering that the stresses in the EL and SML are the same during compression,

$$\sigma_{SML}(\varepsilon_{SML}^{c*}) = \sigma_{EL}(\varepsilon_{EL}^{c*}) \rightarrow E_{EL}^f(\varepsilon_{EL}^{c*})\varepsilon_{EL}^{c*} = E_{SML}^f(\varepsilon_{SML}^{c*})\varepsilon_{SML}^{c*}. \tag{A.3}$$

Expressing ε_i^{c*} with t_i^c and t_i^f, $(i = EL,\ SML)$,

$$E_{EL}^f(\varepsilon_{EL}^{c*})\frac{t_{EL}^c - t_{EL}^f}{t_{EL}^f} = E_{SML}^f(\varepsilon_{SML}^{c*})\frac{t_{SML}^c - t_{SML}^f}{t_{SML}^f}. \tag{A.4}$$

From Eqs. (A.1) and (A.4), we obtain Eqs. (1) – (3).

References

(1) Fung, Y.C., Biomechanics: Motion, Flow, Stress, and Growth, (1990), pp.388–394, Springer-Verlag, New York.

(2) Vaishnav, R.N. and Vossoughi, J., Estimation of Residual Strains in Aortic Segments, in Biomedical Engineering II, Recent Developments, edited by Hall, C.W., (1983), pp.330–333, Pergamon Press, New York.

(3) Fung, Y.C., Biodynamics: Circulation, (1984), pp.54–66, Springer-Verlag, New York.

(4) Wolinsky, H. and Glagov, S., A Lamellar Unit of Aortic Medial Structure and Function in Mammals, Circ. Res., Vol.20 (1967), pp.99–111.

(5) Fung, Y.C., Bio-Viscoelastic Solids, Biomechanics, (1981), pp.196–214, Springer-Verlag, New York.

(6) Matsumoto, T., Sato, J., Yamamoto, M. and Sato, M., Smooth Muscle Cells Freshly Isolated from Rat Thoracic Aortas Are Much Stiffer than Cultured Bovine Cells: Possible Effect of Phenotype, JSME Int. J., Ser. C, Vol.43 (2000), pp.867–874.

(7) Matsumoto, T., Goto, T., Furukawa, T. and Sato, M., Residual Stress and Strain in the Lamellar Unit of the Porcine Aorta: Experiment and Analysis, J. Biomech., (in press).

(8) Matsumoto, T. and Hayashi, K., Analysis of Stress and Strain Distributions in Hypertensive and Normotensive Rat Aorta Considering Residual Strain, ASME J. Biomech. Engng., Vol.118 (1996), pp.62–73.

(9) Chuong, C.J. and Fung, Y.C., On Residual Stresses in Arteries, ASME J. Biomech. Engng., Vol.108 (1986), pp.189–192.

(10) Vossoughi, J., Hedjazi, Z. and Borris, F.S., II., Intimal Residual Stress and Strain in Large Arteries, 1993 Bioengng. Conf., (1993), pp.434–437, ASME, New York.

(11) Greenwald, S., Moore, J.J., Rachev, A., Kane, T. and Meister, J., Experimental Investigation of the Distribution of Residual Strains in the Artery Wall, J. Biomech. Eng., Vol.119 (1997), pp.438–444.

(12) Rachev, A., Theoretical Study of the Effect of Stress-Dependent Remodeling on Arterial Geometry under Hypertensive Conditions, J. Biomech., Vol.30 (1997), pp.819–827.

(13) Matsumoto, T. and Sato, M., Analysis of Stress and Strain Distribution in the Artery Wall Consisted of Layers with Different Elastic Modulus and Opening Angle, JSME Int. J., Ser. C, Vol.45 (2002), pp.906–912.

(14) Wasano, K. and Yamamoto, T., Tridimensional Architecture of Elastic Tissue in the Rat Aorta and Femoral Artery—a Scanning Electron Microscope Study, J. Electron. Microsc., Vol.32 (1983), pp.33–44.